Storage of Hydrogen at 303 K in Graphite Slitlike Pores from Grand Canonical Monte Carlo Simulation

Piotr Kowalczyk,*,†,‡ Hideki Tanaka,† Robert Hołyst,‡ Katsumi Kaneko,† Takumi Ohmori,† and Junichi Miyamoto†

Department of Chemistry, Faculty of Science, Chiba University, 1-3 Yayoi, Chiba, 263, Japan, and Department III, Institute of Physical Chemistry, Polish Academy of Science, Kasprzaka Street 44/52, 01-224 Warsaw, Poland

Received: June 1, 2005; In Final Form: July 6, 2005

Grand canonical Monte Carlo (GCMC) simulations were used for the modeling of the hydrogen adsorption in idealized graphite slitlike pores. In all simulations, quantum effects were included through the Feynman and Hibbs second-order effective potential. The simulated surface excess isotherms of hydrogen were used for the determination of the total hydrogen storage, density of hydrogen in graphite slitlike pores, distribution of pore sizes and volumes, enthalpy of adsorption per mole, total surface area, total pore volume, and average pore size of pitch-based activated carbon fibers. Combining experimental results with simulations reveals that the density of hydrogen in graphite slitlike pores at 303 K does not exceed 0.014 g/cm^3, that is, 21% of the liquid-hydrogen density at the triple point. The optimal pore size for the storage of hydrogen at 303 K in the considered pore geometry depends on the pressure of storage. For lower storage pressures, $p < 30$MPa, the optimal pore width is equal to a 2.2 collision diameter of hydrogen (i.e., 0.65 nm), whereas, for $p \cong 50$MPa, the pore width is equal to an approximately 7.2 collision diameter of hydrogen (i.e., 2.13 nm). For the wider pores, that is, the pore width exceeds a 7.2 collision diameter of hydrogen, the surface excess of hydrogen adsorption is constant. The importance of quantum effects is recognized in narrow graphite slitlike pores in the whole range of the hydrogen pressure as well as in wider ones at high pressures of bulk hydrogen. The enthalpies of adsorption per mole for the considered carbonaceous materials are practically constant with hydrogen loading and vary within the narrow range $q_{st} \cong 7.28-7.85$ kJ/mol. Our systematic study of hydrogen adsorption at 303 K in graphite slitlike pores gives deep insight into the timely problem of hydrogen storage as the most promising source of clean energy. The calculated maximum storage of hydrogen is equal to ≈1.4 wt %, which is far from the United States Department of Energy (DOE) target (i.e., 6.5 wt %), thus concluding that the total storage amount of hydrogen obtained at 303 K in graphite slitlike pores of carbon fibers is not sufficient yet.

1. Introduction

The study of hydrogen adsorption in carbonaceous porous materials has been recently an area of active experimental and theoretical research.[1−6] It is connected with an interest in the development of (transportable) reversible systems for hydrogen storage with high capacity, which is critical to the large scale application of hydrogen fuel cells, in particular for mobile applications. Many researchers focus mostly on liquid-hydrogen (i.e., compression of supercritical hydrogen) and metal-hydrate systems (i.e., chemisorption of hydrogen in metal hydrides), which both have a low energy efficiency.[7−9] Using a suitable adsorbent seems to be a very promising method adopted for hydrogen storage at room temperature. Physical adsorption of hydrogen is interesting due to the possibility of obtaining high storage under normal conditions and relatively low pressure by the adoption of highly uniform microporous materials.[10,11] Furthermore, this storage technique is much safer and cheaper in comparison to the compression or liquefaction of hydrogen. The key problem connected with physical adsorption is to obtain the high value of supercritical hydrogen storage.[12,13] Thus, the adsorbent designed for the storage of hydrogen should be safe, light, cheap, and of course should have a high adsorption capacity. To obtain a suitable driving range of automotive applications, the United States Department of Energy (DOE) target has been set to 6.5 wt % for 2010, which equals 720 mL (STP)/g of an adsorbent. The ultimate 2015 target is more demanding at 9 wt %.

To obtain the high efficiency of hydrogen storage, a new breed of materials, that is, superactivated carbons, activated carbon fibers, carbon monoliths, single-walled carbon nanotubes, single-walled carbon nanohorns, and organic−inorganic hybrid porous complexes, characterized by their high adsorption capacity, hydrophobic nature, and high adsorption/desorption rate are studied.[14−17] The above-mentioned materials predominantly consist of pores of molecular dimensions. Such nanospaces can produce a high packing density of supercritical hydrogen. The search for a suitable material for the alternative fuel storage is currently an active area of research.[18−20] New synthesis techniques have opened the door to designing materials with specific architectures to yield desired properties.

* To whom correspondence should be addressed. E-mail: kowal@kora.ichf.edu.pl.
† Chiba University.
‡ Polish Academy of Science.

10.1021/jp0529063 CCC: $30.25
Published on Web 08/23/2005

Fundamental studies of molecular processes involved in hydrogen adsorption and release are needed to enable the design of improved materials.[21,22] Theory and computation may be used not only for the interpretation of experimental results but also to provide better insight into the adsorption mechanism.[23,24] Proper models of the adsorption system provide a basis for understanding the adsorption behavior and for predicting the type of materials and conditions for efficient hydrogen storage. Modeling of the physical adsorption of hydrogen is a difficult problem due to two main reasons: the supercritical state of hydrogen at room temperature and quantum effects.[25] The supercritical densification of fluid in a confined geometry is different from the physical adsorption of gas under subcritical conditions.[26−28] Briefly, the adsorption of supercritical fluids is generally monomolecular (it also can occur beyond the first layer if the pressure is high enough), and the condensed phase never surrounds the porous medium. At higher pressures, the molecules in nanopores tend to form clusters of irregular shapes.[29,30] As has been shown by many researchers, the adsorption of supercritical fluids, when plotted as the surface excess of adsorption versus pressure for temperatures close to the critical temperature, exhibits a maximum at a pressure close to the critical one; especially when the temperature is slightly greater than the critical temperature, the maximum behaves like a very sharp spike.[31] It is well documented that the potential energies generated by pore walls, temperature, dimension, and shape of the pore have an impact on the position and shape of the surface excess maximum.[32,33]

Due to the small mass of hydrogen and the confinement of the molecules inside the nanospaces, the quantum effects are expected to contribute significantly to the adsorption process. Quantum effects strongly depend on the temperature of storage and density of the stored fluid. For atomic systems, a simple test of the classical hypothesis is obtained by calculating the de Broglie thermal wavelength, Λ, defined as[34]

$$\Lambda = (2\pi\beta\hbar^2/m)^{1/2} \quad (1)$$

where $\beta = (k_b T)^{-1}$, $\hbar = h/2\pi$, m is the mass of an atom, h denotes Planck's constant, k_b is Boltzmann's constant, and T denotes temperature. To justify a classical treatment of static properties, it is necessary that $\Lambda/a \ll 1$, where $a \cong \rho^{-1/3}$ is the mean nearest-neighbor separation. For argon at the triple point ($T = 83.8$ K), $\Lambda = 0.03$ nm and $\Lambda/a = 0.084$. In contrast, for hydrogen at the triple point ($T = 13.8$ K), $\Lambda = 0.33$ nm and $\Lambda/a = 0.94$. From these simple calculations, we recognized that for hydrogen the quantum effects at the triple point cannot be neglected. For a temperature of interest, that is, $T = 303$ K, the de Broglie thermal wavelength for hydrogen in graphite slitlike pores decreases up to 0.07 nm and $\Lambda/a = 0.12$. Here, the density of hydrogen in graphite slitlike pores at 303 K was taken from the current computations as being equal to $\rho = 0.014$ g/cm^3. As one can see, quantum effects for the case of the hydrogen adsorbed in graphite slitlike pores at 303 K are reduced; however, they are still far from the condition given above.

Rzepka et al.[35] have investigated the storage capacity of microporous carbon and carbon nanotubes both theoretically and experimentally. The authors showed that at room temperature a graphite slitlike pore of a size comparable to two hydrogen collision diameters was predicted to be optimal for hydrogen storage. For this configuration at 10 MPa, a maximum storage capacity of 1.3 wt % or 14 kg/m^3 was predicted. Moreover, only for low hydrogen pressures, a cylindrical geometry like that in carbon nanotubes can exceed the storage density of carbon slitlike pores owing to enhanced adsorbate-adsorbent interaction. It is worth pointing out that Rzepka et al. did not incorporate the quantum effects for both adsorbate−adsorbate and adsorbate−adsorbent interactions in all simulations performed in the grand canonical ensemble.

Wang and Johnson[36] employed rigorous path integral grand canonical Monte Carlo (PIGCMC) simulations to compare the adsorption of hydrogen in single-walled carbon nanotubes (SWNTs) with idealized graphite carbon slitlike pores. Although the adsorption potential was enhanced for SWNTs relative to slitlike pores of the same size, the calculations predicted that the storage capacity for an array of nanotubes was less then that of slitlike pores at both 77 and 298 K. The low values of adsorption are mainly a result of the excluded surface area in a close-packed array of tubes and excluded volume in an isolated single carbon tube. Adsorption isotherms were in reasonably good agreement with the experimental data for AX-21 activated carbon but did not account for high storage capacities in carbon nanotubes. It is worth noting that the authors approximated the real pore size distribution of AX-21 activated carbon by a single slitlike pore of average size; hence, this theoretical prediction should be taken as a first approximation. Wang and Johnson pointed out that quantum effects are important even at 298 K for adsorption in tube interstices.

Another study by Darkrim et al.[37] employed Monte Carlo simulations to study hydrogen adsorption on graphite basal planes and in slitlike pores at 293 K. The authors recognized the qualitative agreement between molecular simulation and experimental data on AX-21 activated carbon. Moreover, it was shown that the adsorbent model plays an important role in the comparison of simulation results with the experimental ones. The authors obtained the best agreement modeling the basic unit of activated carbon as a finite stack of graphite planes.

Jagiello and Thommes[38] applied hydrogen adsorption at 77 K to study the distribution of pore sizes in the range of the smallest graphite slitlike pores inaccessible to the other adsorbates. The authors modeled the confined quantum fluid by classical nonlocal density functional theory (NDFT) due to Tarazona's proposal. As shown by Nguyen et al.[39] for very small graphite slitlike pores ($H < 0.351$ nm), the NDFT approach slightly underpredicts the adsorbed phase density of classical fluid in comparison to the GCMC approach. Such deviations being the consequence of the mean-field approximation overpredict the adsorbed amount in the smallest pores and influence the pore size analysis. Additionally, Jagiello and Thommes neglected the quantum effects for both fluid−fluid and solid−fluid interactions in ultra graphite slitlike pores (approximately a pore width lower than 0.3 nm). Moreover, the description of the method applied by the mentioned authors is unclear and incomplete.

In another interesting study of hydrogen isotope adsorption, Tanaka et al.[40] showed that single-walled carbon nanohorns (SWNHs) seem to be suitable materials for hydrogen and deuterium separation due to quantum effects. The authors obtained good agreement between the simulation in the grand canonical ensemble corrected for quantum effects and the experimental data of hydrogen and deuterium adsorption at 77 K in single-walled carbon nanohorns. The quantum effects cause the density of hydrogen inside SWNHs at 77 K to be 8−26% smaller than that of deuterium. The authors pointed out that quantum effects on hydrogen adsorption depend on the pore structures and they are very important even at 77 K.

The purpose of the present manuscript is to model the adsorption of hydrogen at 303 K by grand canonical Monte Carlo (GCMC) simulations. To take into account the quantum

effects in the nature of both adsorbate−adsorbate and adsorbate−adsorbent interactions, the method of effective potential due to Feynman and Hibbs is applied. In quantum corrected GCMC simulations, we collect the excess of adsorption, absolute value of adsorption, enthalpy of adsorption per mole, and one-dimensional center-of-mass to center-of-mass local density profiles between Gaussian packets for hydrogen at 303 K. Finally, we analyze adsorption data of hydrogen at 303 K on different samples of pitch-based activated carbon fibers. Using the concept of the adsorption integral equation, we determine the total storage amount of hydrogen, total pore volume, total surface area, enthalpy of adsorption per mole, and pore size distribution of the above-mentioned carbonaceous materials. We show that the hydrogen density in pores does not exceed 0.014 g/cm^3, that is, 21% of the liquid-hydrogen density at the triple point. Consequently, the adsorption of hydrogen is very weak even at very high pressures, $p = 80$ MPa. The calculated maximum storage of hydrogen is equal to ≈1.4 wt %, which is far from the DOE target, thus concluding that the total storage amount of hydrogen obtained at 303 K in graphite slitlike pores of the investigated carbon fibers is not sufficient to employ these materials as an efficient storage medium under the considered conditions.

2. Description of the Model

In the simulation of supercritical hydrogen adsorption in the graphite slitlike micropores, the grand canonical ensemble (i.e., fixed system of volume, V, temperature, T, and the chemical potential of the bulk fluid, μ_p) was used.[41,42]

To take into account the quantum effects, all simulations were performed for hydrogen in the graphite slitlike pores interacting via the truncated Feynman and Hibbs (FH) effective potential[43,44]

$$V_{FH}^{ff}(r) = \left\{\sum_{n=0}^{k}\frac{1}{n!}\left(\frac{\beta\hbar^2}{24\mu_m}\right)^n \nabla^{2n}[V_{ff}(r)]\right\}\Theta(r_{cut} - r) \quad (2)$$

where r is the distance between two interacting fluid molecules, $\beta = (k_bT)^{-1}$, $\hbar = h/2\pi$, $\mu_m = m/2$ is the reduced mass of a pair of interacting fluid molecules, h denotes Planck's constant, k_b is Boltzmann's constant, and Θ is the Heaviside function. Note that according to eq 2 the quantum fluid molecule is represented by a Gaussian wave packet of width $\hbar/(12mk_bT)^{1/2}$, so the FH effective potential is an average of classical potential over the Gaussian wave packet.

According to Sese,[45,46] for better approximation of the rigorous path integral Monte Carlo (PIMC) simulation, the series given by eq 2 should be cut off at $k = 1$. As a result, the final formula for the calculation of the fluid−fluid interactions is given by the second-order Feynman−Hibbs effective potential

$$V_{FH}^{ff}(r) = \left\{V_{ff}(r) + \left(\frac{\beta\hbar^2}{24\mu_m}\right)\left[\frac{d^2}{dr^2}V_{ff}(r) + \frac{2}{r}\frac{d}{dr}V_{ff}(r)\right]\right\}\Theta(r_{cut} - r) \quad (3)$$

where the classical potential is represented by the one-center Lennard-Jones equation

$$V_{ff}(r) = 4\epsilon_{ff}\left[\left(\frac{\sigma_{ff}}{r}\right)^{12} - \left(\frac{\sigma_{ff}}{r}\right)^{6}\right] \quad (4)$$

Here, σ_{ff} denotes the LJ fluid−fluid collision diameter, ϵ_{ff} is the LJ fluid−fluid potential well depth, and $r_{cut} = 5\sigma_{ff}$ is the cutoff distance. For hydrogen, we used $\sigma_{ff} = 0.2958$ nm and $\epsilon_{ff}/k = 36.7$ K.[47] Here, we want to emphasize that spherical symmetry of the adopted Lennard-Jones potential may not be adequate for the case of high density and low temperature.

According to Sese's PIMC studies, the second-order Feynman−Hibbs (FH) effective potential can be used when the systems are under usual density and the reduced de Broglie thermal wavelength if $\Lambda^* \equiv h/(2\pi mk_bT\sigma_{ff}^2)^{1/2} \leq 0.5$. The Λ^* value for hydrogen in graphite slitlike pores at 303 K is 0.24. Thus, at the considered temperature, the FH method should reproduce the results obtained from the rigorous path integral simulation in the grand canonical ensemble.

The quantum corrected interactions between the hydrogen and single graphite lattice plane of surface density $\rho_s = 38.19$ nm^{-2} is calculated from the equation derived by Tanaka[48]

$$V_{FH}^{sf}(z) = V_{10-4}^{sf}(z) + V_{qu}^{sf}(z) \quad (5)$$

where the classical and quantum terms are given by, respectively,

$$V_{10-4}^{sf}(z) = 2\epsilon_{sf}\pi\rho_s\sigma_{sf}^2\left[\frac{2}{5}\left(\frac{\sigma_{sf}}{z}\right)^{10} - \left(\frac{\sigma_{sf}}{z}\right)^{4}\right] \quad (6)$$

$$V_{qu}^{sf}(z) = 176\epsilon_{sf}\pi\rho_s\frac{\beta\hbar^2}{24\mu}\left[\frac{1}{2}\left(\frac{\sigma_{sf}}{z}\right)^{12} - \frac{1.0}{4.4}\left(\frac{\sigma_{sf}}{z}\right)^{6}\right] \quad (7)$$

Here, z denotes the distance from the hydrogen molecule to the solid surface. Equation 6 is the classical 10−4 potential derived by Steele,[49] whereas eq 7 represents the quantum correction. In eq 7, we used $\mu_m = m$ for the quantum interaction between hydrogen and carbon atoms because we assumed that the carbon atoms in the single graphite plane are linked together rigidly. The solid−fluid parameters were calculated from the Lorentz−Berthelot mixing rule[47]

$$\sigma_{sf} = (\sigma_{ff} + \sigma_{ss})/2 \quad (8)$$

$$\epsilon_{sf} = (\epsilon_{ff}\epsilon_{ss})^{1/2} \quad (9)$$

The LJ parameters for carbon are $\sigma_{ss} = 0.34$ nm and $\epsilon_{ss} = 28$ K.[50]

The results of X-ray diffraction and transmission electron microscopy (TEM) studies indicate that the basic unit, that is, stack of graphite planes, is not infinite.[51,52] Moreover, the influence of the number of graphite planes in the stack of graphite planes above three is negligible for the solid−fluid potential given by eq 5. For this reason, in the current work, we assume that the single slab of graphite wall consists of four basal planes of graphite separated by a uniform spacing of $\Delta = 0.335$ nm.[53] Consequently, the full external potential is written as[54,55]

$$V_{ext}^{sf}(z) = \sum_{j=0}^{3}V_{FH}^{sf}(z + j\Delta) + \sum_{j=0}^{3}V_{FH}^{sf}(H - z - j\Delta) \quad (10)$$

where H is the pore width defined as the distance between the plane passing through all carbon atom centers of the outermost layer of the one wall and the corresponding plane of the opposite wall.

During simulation in the grand canonical ensemble, we collect the average surface excess of hydrogen[56]

$$\Gamma_{av} = \frac{\langle N\rangle - \rho_bL_xL_y(H - \sigma_{ss})}{2L_xL_y} \quad (11)$$

where $\langle N\rangle$ is the ensemble average of the number of molecules in the simulation box, ρ_b is the bulk molecular density, and L_x and L_y are the box lengths in the x and y directions, respectively.

Additionally, we store the average absolute value of hydrogen adsorption defined by the following formula

$$Z_{av} = \frac{\langle N\rangle}{2L_xL_y} \tag{12}$$

The one-dimensional center-of-mass to center-of-mass local density profiles between Gaussian packets are calculated from

$$\rho(z) = \frac{\langle \Delta N(z)\rangle}{\Delta z} \tag{13}$$

Here, $\langle \Delta N(z)\rangle$ is the average number of hydrogen molecules whose centers of mass are located in the segment having boundaries at z and $z + \Delta z$.

By analogy of the enthalpy per mole of the phase transition, the heat released during adsorption in pores is calculated from[57]

$$\frac{q_{st}}{N_A} = \frac{5}{2}k_bT - \frac{\langle EN\rangle - \langle E\rangle\langle N\rangle}{\langle N^2\rangle - \langle N\rangle^2} \tag{14}$$

where $\langle ...\rangle$ denotes the ensemble average, N_A is Avogadro's number, and E is the sum of the kinetic and potential energies.

According to the Feynman−Hibbs model, the total energy is given by[40,45,46]

$$E = \frac{3}{2}\langle N\rangle k_BT + \sum_{i<j}^{N}\beta\left\langle\frac{dV_{FH,ij}^{ff}}{d\beta}\right\rangle + \sum_{i}^{N}\beta\left\langle\frac{dV_{FH,i}^{sf}}{d\beta}\right\rangle + \sum_{i<j}^{N}\langle V_{FH,ij}^{ff}\rangle + \sum_{i}^{N}\langle V_{FH,i}^{sf}\rangle \tag{15}$$

where V_{FH}^{ff} and V_{FH}^{sf} respectively are the fluid−fluid and solid−fluid interaction potentials based on the FH effective potential, N is the number of adsorbed molecules in the simulation box, and $\beta = (k_bT)^{-1}$. The first term of the right-hand side of eq 15 is the kinetic energy of classical molecules, the second and third terms are required by the thermodynamic consistency, and the remaining terms are the potential energies.

To make a comparison with the experimental data, we constructed the distribution of slitlike pore sizes according to the concept of the integral equation[58,59]

$$\Gamma(\rho_b) = \Sigma\Gamma_{loc}(\rho_b,H_{eff})\, f(H_{eff}) \tag{16}$$

Here, $\Gamma_{loc}(\rho_b,H_{eff})$ is the excess value of adsorption in a graphite slitlike pore of effective pore width $H_{eff} = H - \sigma_{ss}$ calculated from GCMC simulation, $\Gamma(\rho_b)$ denotes the measured total excess of adsorption, and $f(H_{eff})$ is the normalized and positive distribution function giving the distribution of pore sizes. The sum runs over all pore sizes.

Note that in eq 16 we describe the total experimental surface excess as a superposition of the excess of adsorption in pores of different dimensions obtained from computer simulation. *The true value of hydrogen* storage *is not an excess quantity but an absolute one*. Thus, only knowing the detailed form of $f(H_{eff})$, we can calculate the total absolute amount of hydrogen, that is, total storage value, by averaging the absolute value of hydrogen adsorption in different pores, $Z_{loc}(\rho_b,H_{eff})$, obtained from GCMC simulation with $f(H_{eff})$

$$Z(\rho_b) = \Sigma Z_{loc}(\rho_b,H_{eff})\, f(H_{eff}) \tag{17}$$

Similarly, the total enthalpy per mole can be simply calculated from

$$Q_{st}(\rho_b) = \Sigma Q_{loc}(\rho_b,H_{eff})\, f(H_{eff}) \tag{18}$$

where $Q_{loc}(\rho_b,H_{eff})$ denotes the enthalpy per mole in graphite slitlike pore of effective width H_{eff} calculated from GCMC simulation. Clearly, the sums in eqs 17 and 18 run over all pore sizes.

In the current study, the excess part of the chemical potential of hydrogen is calculated in the canonical ensemble according to Widom's particle insertion method.[60] In the canonical ensemble, the fluid−fluid interactions were calculated according to eq 3. The corresponding bulk pressure of hydrogen is computed from the virial theorem.[41] The tail corrections for the energy and pressure were added after simulation in the canonical ensemble.[41] The standard GCMC algorithm was used.[41] The cubic simulation box of size $10\sigma_{ff} \times 10\sigma_{ff} \times z$ was surrounded by periodic boundary conditions in the x and y directions.[42] In the z direction, the simulation box was bounded by the pore walls. The cutoff distance for the computing of the fluid−fluid interactions was equal to $5\sigma_{ff}$. No long-range corrections were applied. Both the pressure and chemical potential of hydrogen calculated in the canonical ensemble were inputs in GCMC simulations. For the path of the isotherms, to mimic experimental procedures, the pores were first considered empty. Simulation runs were performed at gradually increasing chemical potentials, and the resulting configurations at the specified conditions were used to initiate the subsequent calculations at higher chemical potentials. In the grand canonical ensemble for every state and slitlike pore size, 7×10^7 configurations were generated. The first 4×10^7 configurations were discarded to guarantee equilibration, whereas the latter 3×10^7 configurations were used to average the desired thermodynamic properties. Additionally, in all simulations, the one-dimensional center-of-mass to center-of-mass local density profile between Gaussian packets was stored. For arbitrary selected points, the fluctuations in the total energy were stored and analyzed to ensure that the thermodynamic equilibrium was achieved.

We calculated the $f(H_{eff})$ functions from eq 16, using a constrained regularization method.[61−63] We solved the inversion problem of determining the pore size distribution by generating the set of local surface excess isotherms of hydrogen at 303 K at 25 values of H^* from GCMC simulation. The slitlike pore widths were distributed logarithmically from $H^* = 1.93$ to $H^* = 20.0$. The local surface excess isotherms of hydrogen were approximated by cubic spine to obtain the value of the surface excess at the experimental points. We used the L-curve method to select the proper value of the regularization parameter.[61,62] Finally, the computed $f(H_{eff})$ value was used to predict both the true storage of hydrogen at 303 K and the enthalpy of adsorption per mole for all investigated samples of pitch-based activated carbon fibers (see eqs 17 and 18, respectively).

3. Experimental Section

Supercritical hydrogen adsorption isotherms of pitch-based activated carbon fibers (ACFs) were measured gravimetrically at 303 K up to 10 MPa by the use of a Cahn microbalance (sensitivity 0.1 μg). The high-purity hydrogen gas (99.99999%, Nippon Sanso) was used after purification with a liquid-nitrogen trap. The pretreatment prior to each adsorption measurement was performed at a pressure less than 1 mPa and a temperature of 423 K for 2 h. The buoyancy correction was done using the

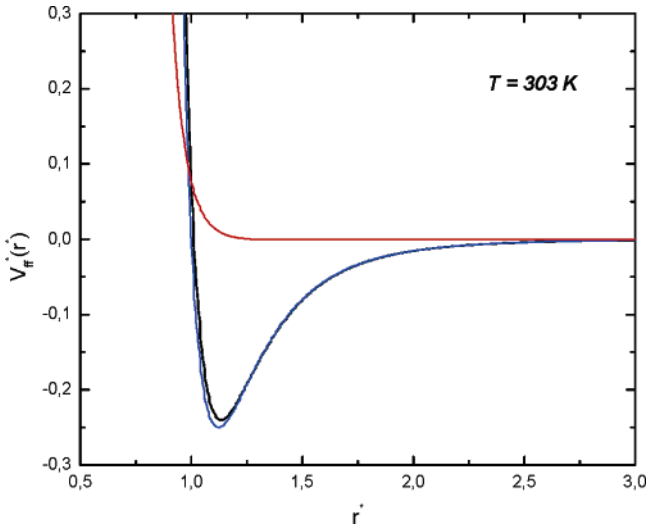

Figure 1. Reduced fluid−fluid interaction potential, $V_{FH}^{ff}(r)/\epsilon_{ff}$, at 303 K: black line, total reduced fluid−fluid interaction potential given by eq 3; blue line, the reduced classical contribution given by eq 4; red line, the reduced quantum contribution.

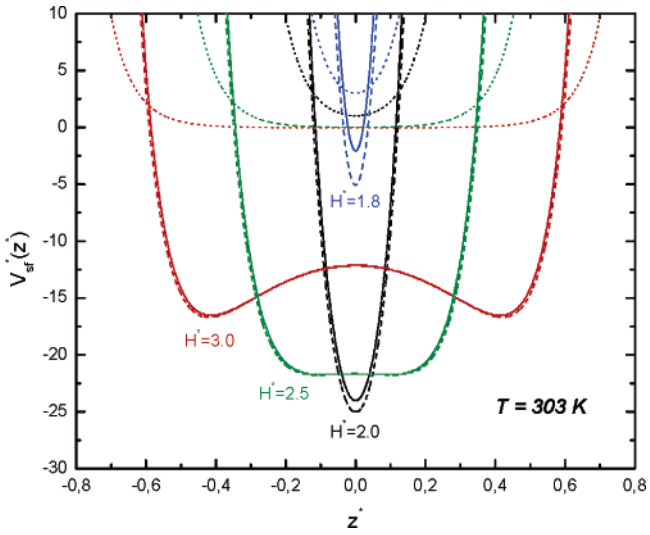

Figure 2. Reduced solid−fluid interaction potential, $V_{ext}^{sf}(z)/\epsilon_{ff}$, for the selected reduced slitlike pore widths, H/σ_{ff}, at 303 K: solid lines, total reduced solid−fluid interaction potential given by eq 10; dashed lines, the reduced classical contributions; dotted lines, the reduced quantum contributions.

particle density of the ACF which was measured by the high-pressure helium buoyancy curve method up to 10 MPa. All remaining details of the experimental measurements can be found elsewhere.[64−65]

4. Results and Discussion

Figure 1 presents the total quantum corrected fluid−fluid interaction potential given by eq 3, classical Lennard-Jones interaction potential for hydrogen given by eq 4, and quantum contribution calculated by the Feynman−Hibbs method. The classical Lennard-Jones interaction potential slightly overestimates the fluid−fluid interaction energy. However, the classical and quantum corrected fluid−fluid interaction potentials are very close to each other at 303 K in the bulk system. For slitlike graphite pores, the differences are much larger (see Figure 2). They are highest for the smallest slitlike graphite pore sizes. An increasing pore size rapidly causes the reduction of the quantum effects.

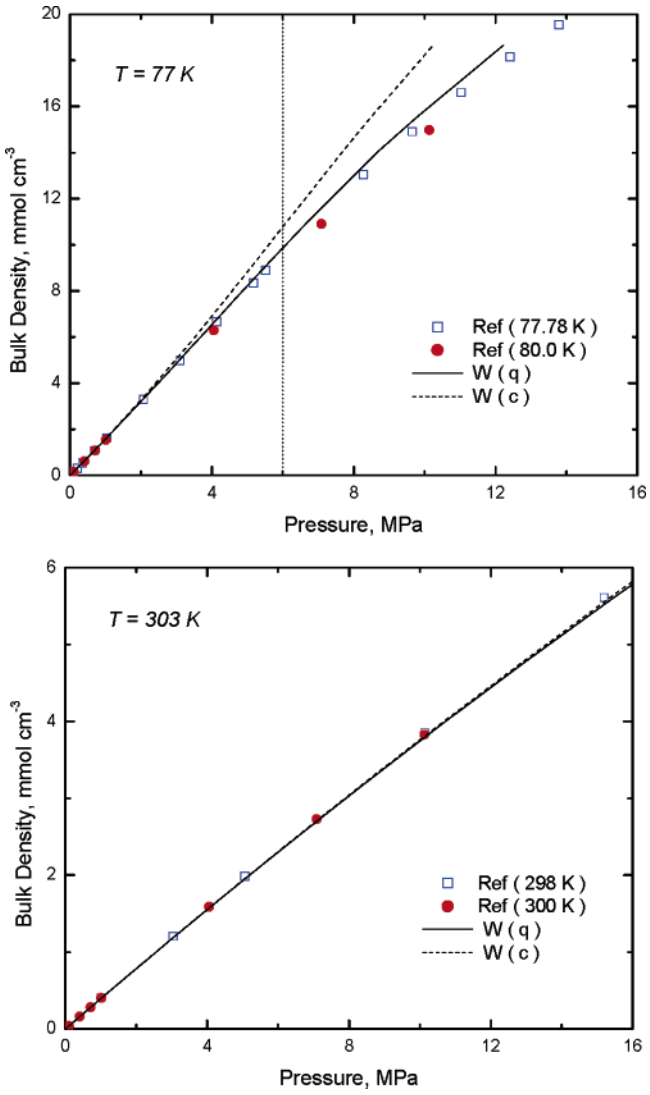

Figure 3. Comparison of the experimental[71] equation of state for hydrogen with the ones obtained from $W(c)$ (simulation of hydrogen treated as classical Lennard-Jones molecules in the canonical ensemble) and $W(q)$ (simulation of hydrogen corrected for quantum effects according to the second-order Feynman−Hibbs effective potential in the canonical ensemble).

Before the systematic study of the hydrogen storage in graphite slitlike pores at 303 K, we checked the consistency of the model of hydrogen−hydrogen interaction in the bulk phase at two temperatures, that is, 77 and 303 K. To capture the experimental region, we select the pressure range up to 16 MPa. The final results are displayed in Figure 3. The key information is the importance of quantum effects for a measuring temperature equal to 77 K. As we see, only the density of bulk hydrogen obtained from simulation in the canonical ensemble corrected for quantum effects according to the Feynman and Hibbs method correlates with experimental data in the whole range of bulk pressures. For 303 K, both the quantum corrected and classical Lennard-Jones model of hydrogen−hydrogen interactions seem to be correct for the prediction of the properties of the bulk hydrogen fluid. Here, we want to emphasize that the quantum effects of fluid placed in nanospaces, that is, in the strong external potential field, cannot be treated as in the bulk phase (see Figures 1 and 2).

Figure 4 presents the selected hydrogen surface excess adsorption isotherms simulated by the GCMC method in graphite slitlike pores of various effective widths at 303 K. The

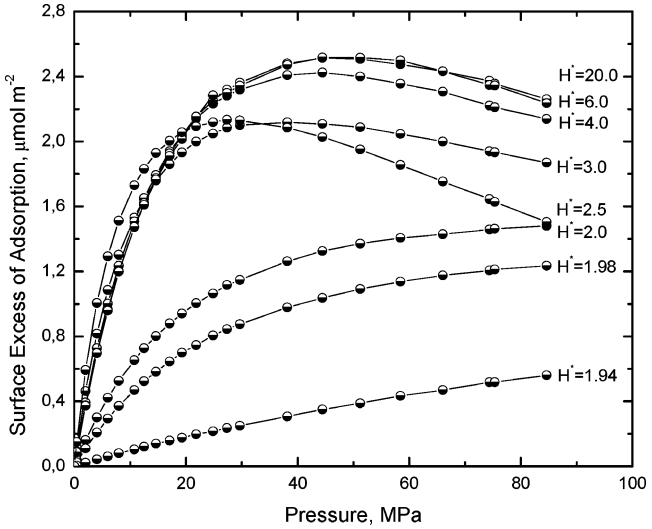

Figure 4. Selected hydrogen surface excess adsorption isotherms simulated by the GCMC method in slitlike graphite pores of various effective widths at 303 K.

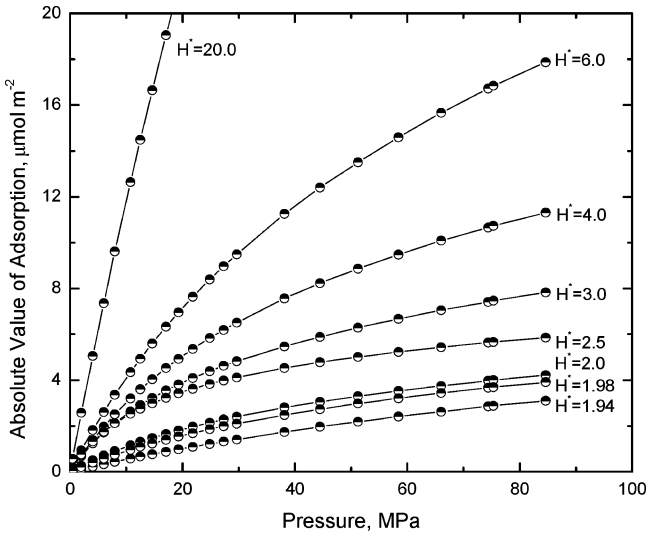

Figure 5. Selected hydrogen absolute adsorbed isotherms simulated by the GCMC method in slitlike graphite pores of various effective widths at 303 K.

maximum on the surface excess isotherm appears for $H^* > 2.05$ in the considered pressure range, that is, up to 85 MPa. For wider pores, the maximum is well developed. The position of the surface excess maximum depends on the size of the pore. Generally, increasing pore size leads to shifting of the surface excess maximum from ≅80 up to ≅50 MPa. Moreover, the packing effect of molecules in the graphite slitlike pore geometry strongly influences both the pressure and value of the surface excess at maximum. However, due to weak hydrogen−graphite interactions at 303 K, the characteristic oscillations disappear very fast (see Figure 6).

Figure 5 displays the absolute value of adsorption in graphite slitlike pores of various sizes. Obviously, for all pores, this function is increasing and the highest value of the absolute amount adsorbed corresponds to the widest pores due to the available space for bulk molecules. The one-dimensional center-of-mass to center-of-mass local density profiles between Gaussian packets for hydrogen at 303 K in graphite slitlike pores are displayed in Supporting Information Figures 6S and 7S. For very small graphite slitlike pores, hydrogen is adsorbed at the

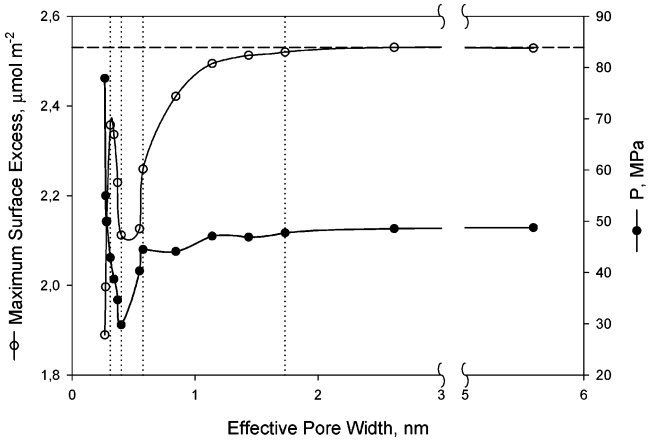

Figure 6. Effect of the effective pore width on the maximum surface excess of adsorption and maximum pressure of hydrogen at 303 K (see Figure 4). The dotted lines denote selected reduced pore widths of H^* = 2.2, 2.5, 3.1, and 7.0 (from left to right).

core of the pore. As one can see from Supporting Information Figure 6S, the density in the core for $H^* = 1.98$ exceeds the corresponding bulk one significantly. Unfortunately, due to strong repulsion between the graphite wall and hydrogen molecules, the excluded volume is large. As a result, the total adsorption is small and the pores of the smallest sizes are not effective for hydrogen storage at 303 K for any considered pressure of the bulk fluid. The maximum surface excess of hydrogen adsorption is observed for graphite slitlike pores of $H^* = 2.2$, since the excluded volume decreases. For graphite slitlike pores of larger sizes, for example, $H^* = 2.5$, the surface excess of hydrogen decreases due to imperfect packing of hydrogen molecules. Next, increasing the pore size causes an increase in the surface excess of hydrogen adsorption up to $H^* \cong 7.2$. For larger pores, the density in the core of the graphite slitlike pore approaches the bulk density and the surface excess of adsorption does not change (see Figures 4 and 6 and Supporting Information Figure 7S). Obviously, we can conclude that the optimal pore size for hydrogen storage at 303 K depends on the storage pressure. For lower storage pressures, $p < 30$ MPa, the optimal pore size corresponds to $H^* = 2.2$, whereas, for $p \cong 50$ MPa, the pore size $H^* \cong 7.2$ seems to be more efficient (see Figure 6).

As one can see in Figures 7 and 8, hydrogen weakly adsorbs in graphite slitlike pores at 303 K. We do not observe a well-defined hexagonal liquidlike structure of the adsorbed layer. Rather, we can recognize a random hard ball type of molecule arrangement. For wider pores and higher pressures of the bulk hydrogen, the appearance of small clusters can be suspected (see Figure 8). As we mentioned above, the adsorption of hydrogen in the considered pore geometry is influenced by the packing effect (see Figures 4 and 6).

Figure 9 presents the dependence of the enthalpy per mole upon hydrogen loading for selected sizes of graphite slitlike pores. At first, the quantum effects depend on the bulk pressure and on the size of the pore. Besides these features, for all pore sizes, the quantum corrected enthalpy of adsorption per mole is always lower than the classical one. Moreover, for pores of the smallest size, the differences between the classical and quantum corrected enthalpy of adsorption per mole are the largest (see Figure 9). Obviously, the general shapes of both above-mentioned dependences are very close to each other, since the lowering of the enthalpy of adsorption per mole at the higher pressures is associated with the building of the adsorbed layers. The lower values of the quantum corrected enthalpy of adsorp-

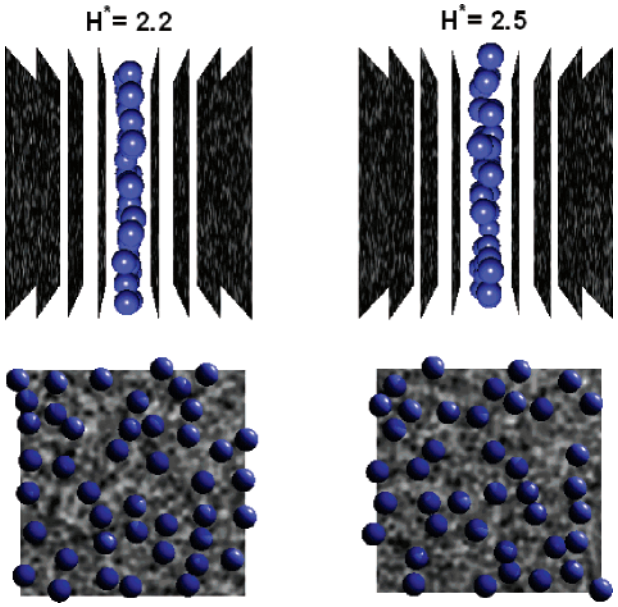

Figure 7. Snapshots of hydrogen at maximum surface excess at 303 K for selected reduced pore widths of $H^* = 2.2$ and 2.5.

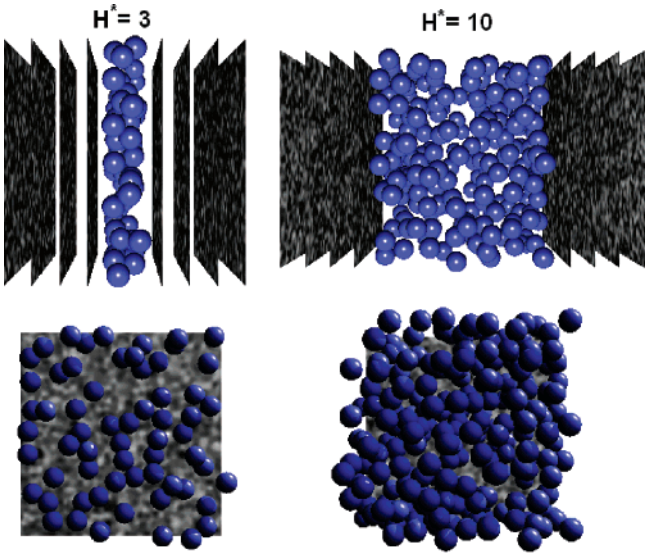

Figure 8. Snapshots of hydrogen at maximum surface excess at 303 K for selected reduced pore widths of $H^* = 3$ and 10.

tion per mole in comparison to the classical one are the result of the lower interaction of quantum hydrogen, that is, the swelling effect being the consequence of the uncertainty principle.

A theoretical description of the experimental excess isotherms of hydrogen at 303 K for several samples of pitch-based activated carbon fibers is displayed in Figure 10 (see panel a). *Please note the excellent agreement between the simulations and the experiment*. We want to point out that nonparametric fitting of experimental data by the regularization method with a suitably chosen value of the regularization parameter does not guarantee agreement between theory and experiment. The good examples were published by Do and Do[66] (see Figure 10) or Ustinov and Do[67] (see Figure 4). Additionally, Figure 10 presents the calculated absolute value of adsorption, that is, the true storage value inaccessible from a gas adsorption experiment (see panel b). Obviously, the true storage value of hydrogen at 303 K does not correspond to the measured surface excess of adsorption and it is always larger. The differences between the

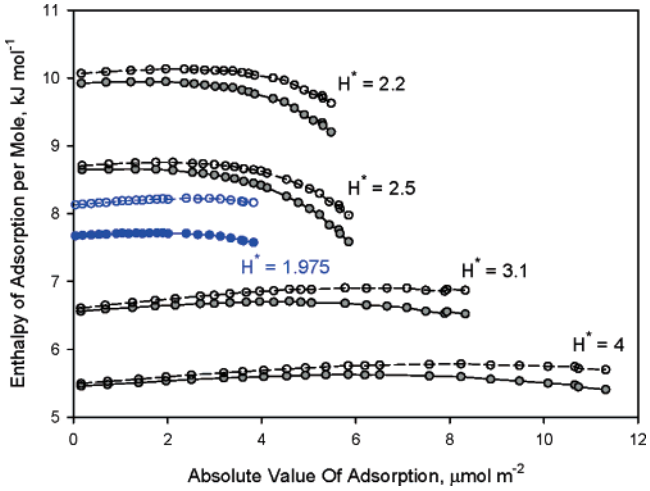

Figure 9. Classical (open circles) and quantum corrected (full circles) enthalpy of adsorption per mole simulated by the GCMC method in slitlike graphite pores of selected reduced pore widths at 303 K.

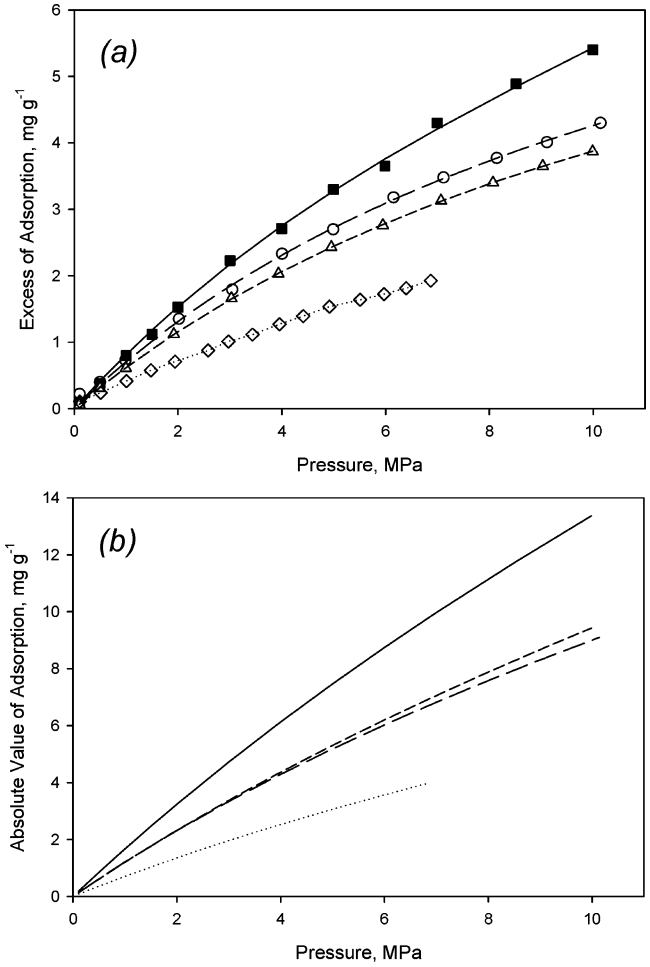

Figure 10. (a) Theoretical description (lines) of experimental excess isotherms (symbols) of hydrogen at 303 K for several samples of pitch-based activated carbon fibers: P5 (diamonds); P15 (triangles); P20 (circles); P25 (rectangles). (b) Calculated absolute value of adsorption of hydrogen at 303 K for the investigated carbon materials.

true storage of hydrogen and the measured surface excess of hydrogen adsorption depend on the distribution of the pore sizes, that is, the internal pore structure of the material.

Figure 11 presents key results of hydrogen storage at 303 K by graphite slitlike activated carbon fibers. The density of hydrogen in the slitlike pores was calculated by dividing the

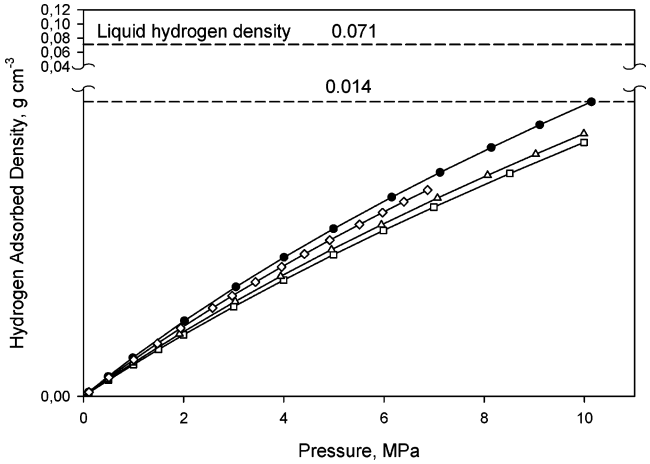

Figure 11. Adsorbed density of hydrogen at 303 K in slitlike graphite pores of pitch-based activated carbon fibers: P5 (diamonds); P15 (triangles); P20 (circles); P25 (rectangles). The liquid-hydrogen density, i.e., $\rho_l = 0.071$ g/cm^3, corresponds to the boiling point ($T = 20.268$ K).

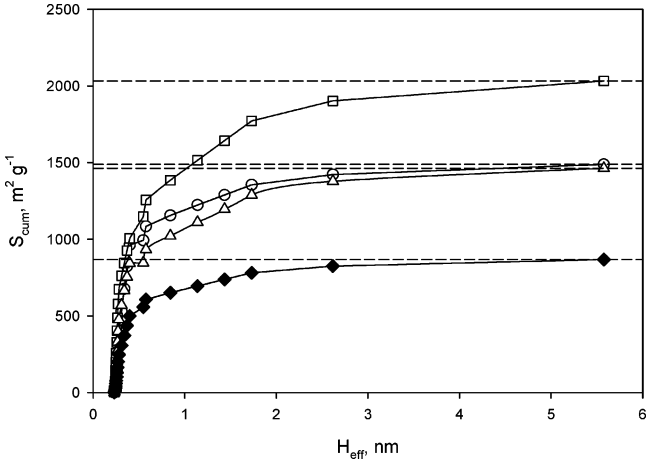

Figure 12. Cumulative pore surface area distribution of the investigated samples of pitch-based activated carbon fibers calculated from hydrogen adsorption at 303 K: P5 (diamonds); P15 (triangles); P20 (circles), P25 (rectangles). The dashed lines denote the total surface area.

TABLE 1: Structural Parameters Calculated from Hydrogen Adsorption Data at 303 K[a]

sample	S_{BET}, m^2 g^{-1}	S_{tot}, m^2 g^{-1}	V_{tot}, cm^3 mol^{-1}	x_{av}, nm	H^*
P5	900[69]	870	0.40	0.34	2.3
P15	1310[69]	1460	0.74	0.32	2.2
P20	1800[69]	1490	0.64	0.33	2.3
P25	1940[70]	2000	1.08	0.33	2.3

[a] Abbreviations: S_{tot}, total surface area; V_{tot}, total pore volume; x_{av}, = H/2.0, average pore size; $H^* = H\sigma_{ff}^{-1}$, reduced pore width. Additionally, the total surface area calculated from a single nitrogen adsorption isotherm at 77 K by the Brunauer, Emmett, and Teller (BET) method was included (S_{BET}).

absolute value of adsorption by the total pore volume of the investigated pitch-based ACF (this is the space in which hydrogen can be adsorbed). The total pore volumes were calculated from the experimental excess isotherms of hydrogen at 303 K and displayed in Table 1. Additionally, in Table 1, we can find the correlation between the surface areas of the investigated carbon materials calculated from nitrogen adsorption at 77 K by the Brunauer, Emmett, and Teller (BET) method and the current proposal. We see that the density of hydrogen in pores corresponds to 21% of the liquid-hydrogen density at the triple point. This state of hydrogen is not sufficient for application of the activated carbon fibers as a storage medium in modern technology, obviously, if we take into account the present storage conditions.

Figure 12 and Supporting Information Figure 8S present the cumulative distribution of the pore sizes and volumes. Table 1 collects the structural data calculated from supercritical hydrogen at 303 K. As one can see, the samples of the investigated pitch-based activated carbon fibers are characterized by different total surface areas and pore volumes, whereas the predicted mean pore size is almost constant. As we mentioned above, this is an optimal pore size for hydrogen storage in the considered experimental range of pressures and temperatures. In conclusion, the main storage of hydrogen at 303 K is with the graphite slitlike pores of $H^* \cong 2.2-2.3$.

The enthalpy of adsorption per mole calculated from experimental data and GCMC simulation is shown in Supporting Information Figure 9S. The shape of the released heat of adsorption is very similar for all of the investigated samples of pitch-based activated carbon fibers. On the other hand, the numerical values are varying from sample to sample, that is, $q_{st} \cong 7.28-7.85$ kJ/mol. Such differences result from the structural and energetic heterogeneity of the considered materials. We should take into account that the enthalpy of adsorption per mole is very sensitive to any surface irregularities, distribution of pore sizes, presence of various chemical groups on the graphite surfaces, and so forth. For these reasons, the enthalpy of adsorption per mole (equal to $q_{st} \cong 10$ kJ/mol) corresponding to average pore width is shifted to a lower value.

Summing up our results, we want to emphasize the importance of quantum effects in the adsorption of hydrogen at 303 K. As we showed, quantum effects can be neglected in the bulk phase due to the relatively high temperature (see Figures 1 and 3); however, in the smallest pores, the quantum corrected enthalpy of adsorption per mole is significantly shifted compared with the classical one (see Figures 2 and 9). Moreover, for larger sizes of graphite slitlike pores at the high pressure of the bulk hydrogen, quantum effects can also be very important even with a weaker confinement effect. The optimal pore size of the graphite slitlike pore for hydrogen storage at 303 K depends on the pressure of storage. For lower storage pressures, $p < 30$ MPa, the optimal pore size corresponds to $H^* = 2.2$, whereas, for $p \cong 50$ MPa, the pore size $H^* \cong 7.2$ seems to be more efficient due to the available space accessible for bulk hydrogen molecules (see Figure 6). For the very small graphite slitlike pores, that is, $H^* < 2.2$, the storage of hydrogen is lowered due to the large excluded volume being the result of the strong repulsion between graphite walls and hydrogen molecules (see Figures 4−6 and Supporting Information Figure 6S). The constructed distribution of the pore sizes of several samples of pitch-based activated carbon fibers indicates that the adsorbed density of hydrogen in graphite slitlike pores at 303 K does not exceed 0.014 g/cm^3 (see Figure 11). This value corresponds to 21% of the liquid-hydrogen density at the triple point. The storage value of hydrogen adsorption, that is, the absolute value of hydrogen adsorption, depends on the total surface area and pore volume (compare the results form Table 1 and Figure 10). The description of the experimental excess isotherm of hydrogen indicates that the hydrogen is mainly stored in the pores with sizes corresponding to the optimal one, that is, $H^* \cong 2.2-2.3$, in the considered pressure and temperature ranges (see Table 1). As we observe in Figure 13, the maximum value of hydrogen storage at 303 K in graphite slitlike pores linearly depends on the total surface area of the pitch-based activated carbon fiber.

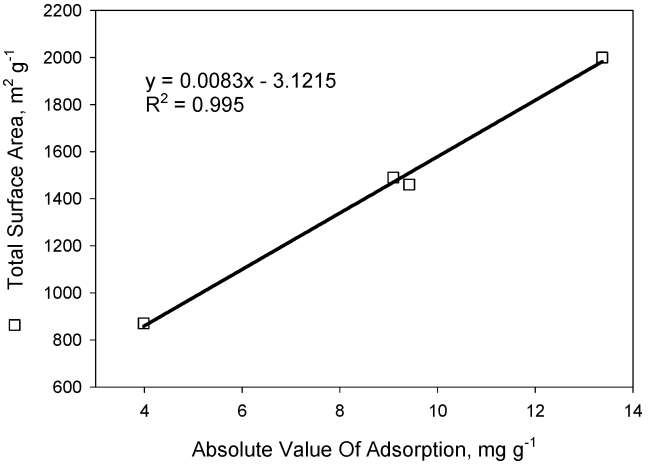

Figure 13. Dependence of the absolute value of hydrogen adsorption at 303 K upon the total surface area. The corresponding gas pressure was 10 MPa.

The calculated maximum storage of hydrogen is equal to ≈1.4 wt %, which is far from the United States Department of Energy (DOE) target (i.e., 6.5 wt %) for 2010. This value corresponds to P25 ACF characterized by a large surface area of ≅2000 m^2/g and mainly composed of graphite slitlike pores of molecular dimension (see Figures 10 and 13). The calculated total storage of hydrogen is close to the experimental results published by de la Casa-Lillo et al.[68] (see Figure 2). Taking into account the current results, we can state that these carbonaceous materials are not an efficient storage medium under the considered conditions.

Acknowledgment. P.K. gratefully acknowledges Dr. A. P. Terzyk (N. Copernicus University, Torun, Poland) for fruitful comments and suggestions considering the current paper. This work is dedicated to Prof. L. Solarz (Military Academy of Technology, Warsaw, Poland). This work was supported by NEDO project (Development of Evaluation Method of Hydrogen Adsorption on Carbons).

Supporting Information Available: Figures showing one-dimensional center-of-mass to center-of-mass local density profiles between Gaussian packets for hydrogen at 303 K in graphite slitlike pores and the cumulative pore volume distribution of and the enthalpy of adsorption per mole for the investigated samples of pitch-based activated carbon fibers. This material is available free of charge via the Internet at http://pubs.acs.org.

References and Notes

(1) Dillon, A. C.; Jones, K. M.; Bekkedahl, T. A.; Kiang, C. H.; Bethune, D. S.; Heben, M. J. *Nature* **1997**, *386*, 377.
(2) Liu, C.; Fan, Y. Y.; Liu, M.; Cong, H. T.; Cheng, H. M.; Dresselhaus, M. S. *Science* **1999**, *286*, 1127.
(3) Dillon, A. C.; Heben, M. J. *Appl. Phys. A* **2001**, *72*, 133.
(4) Nijkamp, M. G.; Raaymakers, J. E. M. J.; van Dillen, A. J.; de Jong, K. P. *Appl. Phys. A* **2001**, *72*, 619.
(5) Chahine, R.; Bose, T. K. *Int. J. Hydrogen Energy* **1994**, *19*, 161.
(6) Carpetis, C.; Peschka, W. *Int. J. Hydrogen Energy* **1980**, *5*, 539.
(7) Schlapbach, L.; Züttel, A *Nature* **2001**, *414*, 353.
(8) Dresselhaus, M. S.; Thomas, I. L. *Nature* **2001**, *414*, 332.
(9) Zaluska, A.; Zaluski, L.; Stroem-Olsen, J. O. *Appl. Phys. A* **2001**, *72*, 157.
(10) Chen, J.; Wu, F. *Appl. Phys. A* **2004**, *78*, 989.
(11) Shao, X.; Wang, W.; Xue, R.; Shen, Z. *J. Phys. Chem. B* **2004**, *108*, 2970.
(12) Murata, K. *Fundamental study of high-pressure adsorption of supercritical gases*; Chiba University: Chiba, Japan, 2001.
(13) Hynek, S.; Fuller, W.; Bentley, J. *Carbon* **1997**, *22*, 6601.
(14) Murata, K.; Kaneko, K.; Kanoh, H.; Kasuya, D.; Takahashi, K.; Kokai, F.; Yudasaka, M.; Iijima, S. *J. Phys. Chem. B* **2002**, *106*, 11132.
(15) Anson, A.; Callejas, M. A.; Benito, A. M.; Maser, W. K.; Izquierdo, M. T.; Rubio, B.; Jagiello, J.; Thommes, M.; Parra, J. B.; Martinez, M. T. *Carbon* **2004**, *42*, 1237.
(16) Züttel, A.; Sudan, P.; Mauron, P.; Wenger, P. *Appl. Phys. A* **2004**, *78*, 941.
(17) Shiraishi, M.; Takenobu, T.; Kataura, H.; Ata, M. *Appl. Phys. A* **2004**, *78*, 947.
(18) Seki, K. *Chem. Commun.* **2001**, 1496.
(19) Duren, T.; Snurr, R. Q. *J. Phys. Chem. B* **2004**, *108*, 15703.
(20) Iijima, S.; Yudasaka, M.; Yamada, R.; Bandow, S.; Suenaga, K.; Kokai, F.; Takahashi, K. *Chem. Phys. Lett.* **1999**, *309*, 165.
(21) Wang, Q.; Johnson, J. K. *J. Phys. Chem. B* **1999**, *103*, 4809;
(22) Tanaka, H.; El-Merraoui, M.; Kanoh, H.; Steele, W. A.; Yudasaka, M.; Iijima, S.; Kaneko, K. *J. Phys. Chem. B* **2004**, *108*, 17457.
(23) Challa, R. S.; Sholl, D. S.; Johnson, J. K. *J. Chem. Phys.* **2002**, *116*, 814.
(24) Cracknell, R. F. *Mol. Simul.* **2001**, *27*, 287.
(25) Stan, G.; Cole, M. W. *J. Low Temp. Phys.* **1998**, *110*, 539.
(26) Do, D. D.; Do, H. D.; Ustinov, E. A. *Langmuir* **2003**, *19*, 2215.
(27) Ustinov, E. A.; Do, D. D. *Langmuir* **2003**, *19*, 8349.
(28) Kowalczyk, P.; Tanaka, H.; Kaneko, K.; Terzyk, A. P.; Do, D. D. *Langmuir* **2005**, *21*, 5639.
(29) Ohba, T.; Omori, T.; Kanoh, H.; Kaneko, K. *J. Phys. Chem. B* **2004**, *108*, 27.
(30) Kowalczyk, P.; Kaneko, K.; Kanoh, H.; Tanaka, H.; Ustinov, E. A. *Abstract of Spring Meeting of Chemical Society of Japan* **2004**, *1*, 308.
(31) Do, D. D.; Do, H. D. *Carbon* **2003**, *41*, 1777.
(32) Tan, Z.; Gubbins, K. E. *J. Phys. Chem. B* **1990**, *94*, 6061.
(33) Jiang, S.; Zollweg, J. A.; Gubbins, K. E. *J. Phys. Chem. B* **1994**, *98*, 5709.
(34) Hansen, J. P.; McDonald, I. R. *Theory of Simple Liquids*; Academic Press: London, 1990.
(35) Rzepka, M.; Lamp, P.; de la Casa-Lillo, M. A. *J. Phys. Chem. B* **1998**, *102*, 10894.
(36) Wang, Q.; Johnson, J. K. *J. Chem. Phys.* **1999**, *110*, 577.
(37) Darkrim, F.; Vermesse, J.; Malbrunot, P. *J. Chem. Phys.* **1999**, *110*, 4020.
(38) Jagiello, J.; Thommes, M. *Carbon* **2004**, *42*, 1227.
(39) Nguyen, T. X.; Bhatia, S. K.; Nicholson, D. *Langmuir* **2005**, *21*, 3187.
(40) Tanaka, H.; Kanoh, H.; Yudasaka, M.; Iijima, S.; Kaneko, K. *J. Am. Chem. Soc.* **2005**, *127*, 7511.
(41) Frenkel, D.; Smit, B. *Understanding Molecular Simulation Form Algorithms To Applications*; Academic Press: London, 1996.
(42) Allen, M. P.; Tildesley, D. J. *Computer Simulation of Liquids*; Clarendon: Oxford, U.K., 1987.
(43) Feynman, R. P.; Hibbs, A. *Quantum Mechanics and Path Integrals*; McGraw-Hill: New York, 1965.
(44) Feynman, R. P. *Statistical Mechanics*; Benjamin: New York, 1972.
(45) Sese, L. M. *Mol. Phys.* **1994**, *81*, 1297.
(46) Sese, L. M. *Mol. Phys.* **1995**, *85*, 931.
(47) Levesque, D.; Gicquel, A.; Darkrim, F. L.; Kayiran, S. B. *J. Phys.: Condens. Matter* **2002**, *14*, 9285.
(48) Tanaka, H. Unpublished results.
(49) Steele, W. A. *The Interaction of Gases with Solid Surfaces*; Pergamon Press: Oxford, U.K., 1974.
(50) Do, D. D. *Adsorption Analysis: Equilibria and Kinetics*; Imperial College Press: London, 1998.
(51) Fryer, J. R. *Carbon* **1980**, *18*, 397. Marsh, H.; Crafword, D. *Carbon* **1982**, *20*, 419.
(52) You, F. Y.; McEnaney, B.; Mays, T. J. *Carbon* **1998**, *36*, 1425.
(53) Lastoskie, Ch.; Gubbins, K. E.; Quirke, N. *Langmuir* **1993**, *9*, 2693.
(54) Crowell, A. D. *J. Chem. Phys.* **1954**, *22*, 1397.
(55) Dobruskin, V. Kh. *Carbon* **2002**, *40*, 659.
(56) Do, D. D.; Do, H. D. *Langmuir* **2004**, *20*, 10889.
(57) Nicholson, D.; Parsonage, N. G. *Computer Simulation and the Statistical Mechanics of Adsorption*; Academic Press: London, 1982.
(58) Rouquerol, F.; Rouquerol, J.; Sing, K. S. W. *Adsorption by Powders and Porous Solids*; Academic Press: New York, 1999.
(59) Sweatman, M. B.; Quirke, N. *Mol. Simul.* **2001**, *27*, 295.
(60) Widom, B. *J. Chem. Phys.* **1963**, *39*, 2808.
(61) Kowalczyk, P.; Tanaka, H.; Kanoh, H.; Kaneko, K. *Langmuir* **2004**, *20*, 2324.
(62) Szombathely, M.v.; Brauer, P.; Jaroniec, M. *J. Comput. Chem.* **1992**, *13*, 17.
(63) Provencher, S. W. *Comput. Phys. Commun.* **1982**, *27*, 213.
(64) Murata, K.; Kaneko, K.; Kanoh, H.; Kasuya, D.; Takahashi, K.; Kokai, F.; Yudasaka, M.; Iijima, S *J. Phys. Chem. B* **2002**, *106*, 11132.
(65) Murata, K.; Yudasaka, M.; Iijima, S.; El-Merraoui, M.; Kaneko, K. *J. Appl. Phys.* **2002**, *92*, 1−3.
(66) Do, D. D.; Do, H. D. *Langmuir* **2003**, *19*, 8302.

(67) Ustinov, E. A.; Do, D. D. *Langmuir* **2004**, *20*, 3791.
(68) De la Casa-Lillo, M. A.; Lamari-Darkrim, F.; Cazorla-Amoros, D.; Linares-Solano, A. *J. Phys. Chem. B* **2002**, *106*, 10930.
(69) Miyawaki, J.; Kanda, T.; Kaneko, K. *Langmuir* **2001**, *17*, 664.
(70) Kaneko, K.; Hanzawa, Y.; Iiyama, T.; Kanda, T.; Suzuki, T. *Adsorption* **1999**, *5*, 7.
(71) Vagraftik, N. B. *The Handbook of Thermodynamic Properties of Gases and Liquids*; G.I.F.M.L.: Moscow, 1963.